IMPACT OF LIDAR SYSTEM CALIBRATION ON THE RELATIVE AND ABSOLUTE ACCURACY OF DERIVED POINT CLOUD

A. Habib [a*], K. Bang [a], A. P. Kersting [a]

[a] Department of Geomatics Engineering, University of Calgary, 2500 University Dr NW, Calgary, Alberta, T2N1N4 Canada - (ahabib, kibang, ana.kersting)@ucalgary.ca

Commission I, WG I/2

KEY WORDS: LiDAR, Calibration, Quality Control, Surface Match

ABSTRACT:

LiDAR is a rapid and effective system to collect 3D surface data. In order to achieve the expected accuracy of LiDAR data, systematic errors in a LiDAR system should be defined and removed by a calibration procedure. In this paper, we consider mounting errors (lever-arm and boresight angles) and systematic errors of a laser scanner (scan mirror angle scale and laser range bias). Those systematic errors cause not only the deterioration of absolute accuracy of point cloud w.r.t. the mapping frame but also discrepancies between overlapping strips. This paper investigates the impact of systematic errors on the positional accuracy of a LiDAR point cloud, and proposes two alternative methods for LiDAR system calibration. The first procedure, denoted as "Simplified method", makes use of the LiDAR point cloud from parallel LiDAR strips acquired by a steady platform (e.g., fixed wing aircraft) over an area with moderately varying elevation. The second procedure, denoted as "Quasi-rigorous method", can deal with non-parallel strips, but requires time-tagged LiDAR point cloud and navigation data (trajectory position only) acquired by a steady platform. The performance of the proposed methods is verified by evaluating the relative and absolute accuracy of the point cloud. The relative accuracy is evaluated through the compatibility comparison for overlapping strips before and after the calibration procedure. The absolute accuracy of the point cloud is evaluated by using the LiDAR data for photogrammetric georeferencing before and after performing the proposed calibration procedures.

1. INTRODUCTION

LiDAR technology has been extensively used for the collection of a high density and accurate topographic data. A LiDAR system is composed of a laser ranging and scanning unit and a position and orientation system (POS). The POS consists of an integrated differential global positioning system (DGPS) and an inertial measurement unit (IMU). The laser scanner measures distances from the sensor to the ground, while the integrated GPS/IMU observations provide the position and attitude information of the scanner.

As a result of the non-transparent and sometimes empirical calibration procedures, collected LiDAR data might exhibit systematic discrepancies between conjugate surface elements in overlapping strips. The elimination and/or reduction of the effect of systematic errors in the system parameters have been the focus of the LiDAR research community in the past few years. The existing approaches can be classified into two main categories: system driven (calibration) and data driven (strip adjustment) methods. This categorization is mainly related to the nature of the utilized data and mathematical model. System driven (or calibration) methods are based on the physical sensor model relating the system measurements/parameters to the ground coordinates of the LiDAR points. These methods incorporate the system's raw data (e.g., Filin, 2001; Morin, 2002; Skaloud and Lichti, 2006; Friess, 2006) or at least the trajectory and time-tagged point cloud (Burman, 2000; Toth, 2002; Habib et. al., 2010a) for the estimation of biases in the system parameters with the help of the LiDAR equation. In this paper, the term "raw data" is used to denote all the quantities present in the LiDAR equation (i.e., position and orientation information as well as the measured range and scan angle for each pulse). Moreover, the utilized sequence of rotation angles defining the system attitude and boresight angles has to be defined. The access to the system raw measurements is usually restricted to LiDAR system manufacturers. Such a restriction

has triggered the development of methods that utilize the XYZ coordinates of the LiDAR point cloud only. These procedures are classified as data-driven (or strip adjustment) methods (Kilian et al., 1996; Crombaghs et al., 2000; Maas, 2002; Bretar et al., 2004; Filin and Vosselman, 2004; Kager, 2004). The major drawback of such methods is the mathematical model employed. The effects of systematic errors in the system parameters are usually modeled by an arbitrary transformation function between the laser strip coordinate system and the reference coordinate system. The utilized transformation function might not be appropriate depending on the nature of the inherent biases in the LiDAR system parameters.

The objective of this paper is to investigate the impact of systematic errors on the relative and the absolute accuracy of the LiDAR point cloud. Also, two alternative calibration procedures based on the use of overlapping LiDAR strips are outlined in this paper and utilized to remove the impact of systematic errors in the LiDAR point cloud. The two presented methods differ in terms of data requirement to satisfy the needs of several users. The first procedure, denoted as the "Simplified method", is designed to work with the LiDAR point cloud only. In spite of the increasing adoption of the LAS format, some of the mapping agencies still require only the delivery of the XYZ coordinates of the LiDAR point cloud. Therefore, several users only have access to the point cloud coordinates. Although the Simplified method has the same data requirement as strip adjustment procedures, it properly models the impact of the present systematic errors on the LiDAR point cloud. The simple nature of the utilized data in the Simplified method requires a strict flight configuration and terrain characteristics. More specifically, the Simplified method assumes the availability of parallel flight lines with small pitch and roll angles as well as minor terrain elevation variations compared to the flying height above ground. The second procedure, denoted as the "Quasi-rigorous method", is designed to work with time-tagged LiDAR point cloud and navigation data (trajectory position). In

contrast to the position and orientation information for each pulse, which is needed for rigorous calibration procedures, the Quasi-rigorous method only requires a sample of the trajectory positions at a much lower rate. The only requirement of this method is having a system with small pitch and roll angles, which is quite realistic for steady platforms (e.g., fixed-wing aircraft). The two proposed methods can be applied in any type of terrain coverage without the need for control surfaces and are relatively easy to implement. Therefore, they can be used in every flight mission if needed. Besides, the proposed procedures require minimal interaction from the user, which can be completely eliminated after minor extension of the suggested procedure.

The paper starts by outlining the proposed calibration procedures. Then, the performance and impact of the calibration procedures on the relative and absolute accuracy of the LiDAR point cloud is evaluated through experimental results from real data. Finally, the paper presents some conclusions and recommendations for future work.

2. LIDAR SYSTEM CALIBRATION METHODS

2.1 Concept

The coordinates of the LiDAR points are the result of combining the derived measurements from each of its system components, as well as the mounting parameters relating such components. The relationship between the system measurements and parameters is embodied in the LiDAR equation (Schenk, 2001; El-Sheimy et al., 2005), Equation 1. The position of the laser point, $\vec{X}_G$, is derived through the summation of three vectors ($\vec{X}_o$, $\vec{P}_G$ and $\vec{\rho}$) after applying the appropriate rotations: $R_{yaw,\ pitch,\ roll}$, $R_{\Delta\omega,\Delta\phi,\Delta\kappa}$ and $R_{\alpha,\ \beta}$. In this equation, $\vec{X}_o$ is the vector from the origin of the ground reference frame to the origin of the IMU coordinate system, $\vec{P}_G$ (lever-arm offset vector) is the offset between the laser unit and IMU coordinate systems (w.r.t. the IMU body frame), and $\vec{\rho}$ is the laser range vector whose magnitude is equivalent to the distance from the laser firing point to its footprint. It should be noted that $\vec{X}_o$ is derived through the GPS/INS integration process while considering the lever-arm offset vector between the IMU body frame and the phase centre of the GPS antenna. The term $R_{yaw,\ pitch,\ roll}$ stands for the rotation matrix relating the ground and IMU coordinate systems – which is derived through the GPS/INS integration process, $R_{\Delta\omega,\Delta\phi,\Delta\kappa}$ represents the rotation matrix relating the IMU and laser unit coordinate systems – which is defined by the boresight angles, and $R_{\alpha,\ \beta}$ refers to the rotation matrix relating the laser unit and laser beam coordinate systems with α and β being the mirror scan angles. For a linear scanner, which is the focus of this research work, the mirror is rotated in one direction only leading to zero α angle. S_α and S_β are the scale factor of the angles measured by the scanner, while $\Delta\rho$ is the systematic error in the measured range. The involved quantities in the LiDAR equation are all measured during the acquisition process except for the boresight angles and lever-arm offset vector (mounting parameters), and the scanner angle scale factors and the range systematic error which are usually determined through a calibration procedure.

$$\vec{X}_G = \vec{X}_o + R_{yaw,\ pitch,\ roll}\left(\vec{P}_G + R_{\Delta\omega,\ \Delta\phi,\ \Delta\kappa}\ R_{S_\alpha\ \alpha, S_\beta\ \beta}\begin{bmatrix} 0 \\ 0 \\ -\rho+\Delta\rho \end{bmatrix}\right) \quad (1)$$

The LiDAR point coordinates ($\vec{X}_G$), as shown in Equation 1, are function of the system parameters ($\vec{x}$) and measurements ($\vec{l}$) (Equation 2) and represent the true point coordinates ($\vec{X}_{True}$). In the presence of biases in the system parameters, the LiDAR point coordinates will become biased ($\vec{X}_{Bias}$) and will be function of the system parameters and measurements as well as the biases in the system parameters $(\delta\vec{x})$, as expressed by Equation 3. In this work, as shown in Equation 2, we will investigate the impact of biases in the lever-arm offset components ($\delta\Delta X, \delta\Delta Y, \delta\Delta Z$), biases in the boresight angles ($\delta\Delta\omega, \delta\Delta\phi, \delta\Delta\kappa$), constant bias in the measured ranges $(\delta\Delta\rho)$, and constant scale bias in the scan mirror angles (δS). Equation 3 can be linearized with respect to the system parameters using Taylor series expansion, yielding the form in Equations 4 and 5, after ignoring second and higher order terms. The term $\partial f\ /\ \partial\vec{x}$ represents the partial derivatives with respect to the system parameters, while the term $\partial f\ /\ \partial\vec{x}\delta\vec{x}$ represents the impact of the system biases onto the derived point cloud $\delta\vec{X}_G$.

$$\vec{X}_G = \vec{X}_{True} = f(\vec{x},\vec{l}\,) \quad (2)$$
where,
$\vec{x} = (\Delta X, \Delta Y, \Delta Z, \Delta\omega,\ \Delta\phi,\ \Delta\kappa, \Delta\rho, S\,)$,
and $\vec{l} = \left(\vec{X}_o, yaw, pitch, roll, \beta, \rho\right)$

$$\vec{X}_{Bias} = f(\vec{x}+\delta\vec{x},\vec{l}\,) \quad (3)$$
where,
$\delta\vec{x} = (\delta\Delta X, \delta\Delta Y, \delta\Delta Z, \delta\Delta\omega,\ \delta\Delta\phi,\ \delta\Delta\kappa, \delta\Delta\rho, \delta S\,)$

$$\vec{X}_{Bias} \approx f(\vec{x},\vec{l}\,) + \frac{\partial f}{\partial\vec{x}}\delta\vec{x} = \vec{X}_{True} + \frac{\partial f}{\partial\vec{x}}\delta\vec{x} = \vec{X}_{True} + \begin{bmatrix} \delta X_G \\ \delta Y_G \\ \delta Z_G \end{bmatrix}_T \quad (4)$$

$$\vec{X}_{Bias} \approx \vec{X}_{True} + \begin{bmatrix} \delta X_G \\ \delta Y_G \\ \delta Z_G \end{bmatrix}_{\delta\Delta X,\delta\Delta Y,\delta\Delta Z,\delta\Delta\omega,\delta\Delta\phi,\delta\Delta\kappa,\delta\Delta\rho,\delta S} \quad (5)$$

In the proposed calibration methods, the system biases are determined by utilizing the observed discrepancies in overlapping strips. Therefore, the mathematical relationship between conjugate points in overlapping strips should be determined. Such relationship can be derived by rewriting Equation 5 for two overlapping strips (A and B) and subtracting the resulting equations from each other, as shown in Equation 6. The mathematical models of the proposed calibration procedures are based on Equation 6. Instead of the LiDAR geometric model in Equation 1, the proposed methods will utilized simplified LiDAR equations, which are derived based on a few assumptions. The particularities of each of the methods are discussed in the following subsections.

$$\vec{X}_{Bias}^A - \vec{X}_{Bias}^B = \begin{bmatrix} \delta X_G \\ \delta Y_G \\ \delta Z_G \end{bmatrix}_T^A - \begin{bmatrix} \delta X_G \\ \delta Y_G \\ \delta Z_G \end{bmatrix}_T^B \quad (6)$$

2.2 Simplified Method

The Simplified method provides a new concept of utilizing estimated discrepancies between conjugate surface elements in

overlapping strips, using the LiDAR point cloud only, for the estimation of biases in the system parameters. More specifically, this calibration method consists of a two-step procedure: first, the discrepancies between parallel overlapping strips are determined; then, the system biases are estimated using the detected discrepancies between the strips.

The following assumptions are considered in the Simplified method: (a) we are dealing with a linear scanner with the mirror scanning in the across-flight direction, (b) flying directions are parallel to the positive and negative directions of the Y-axis of the ground coordinate system, (c) the flight lines follow a straight-line trajectory with constant attitude, (d) the LiDAR system is almost vertical (*i.e.*, $R_{yaw, pitch, roll} \approx$ Identity matrix for a system flying along the positive direction of the Y-axis), (e) the LiDAR system has relatively small boresight angles, (f) the mapped area is comprised of a relatively flat terrain, where height variations are much smaller than the flying height above ground, and (g) the Y-axis of the ground coordinate system is defined half-way between the overlapping strips at the ground level. The convention used for the laser scanner and IMU body frame coordinate systems is right-forward-up (right-handed). Such assumptions simplify the LiDAR geometric model as represented by Equation 1 to the form in Equation 7. Note that the scan angle (β) and the lateral distance (x) for a given point are defined relative to the flight trajectory. Therefore, one should use the appropriate signs when dealing with two flight lines, which are flown in opposite directions. Based on the above assumptions, one can conclude that the Simplified method requires the availability of parallel flight lines captured by a steady platform over an area with moderately varying elevation.

$$\vec{X}_G \approx \vec{X}_o + \begin{bmatrix} \pm \Delta X \\ \pm \Delta Y \\ \Delta Z \end{bmatrix} + \begin{bmatrix} \pm I & \mp \Delta\kappa & \pm \Delta\varphi \\ \pm \Delta\kappa & \pm I & \mp \Delta\omega \\ -\Delta\varphi & \Delta\omega & I \end{bmatrix} \begin{bmatrix} -(\rho + \Delta\rho)\ sin(S\ \beta) \\ 0 \\ -(\rho + \Delta\rho)\ cos(S\ \beta) \end{bmatrix}$$

$$= \vec{X}_o + \begin{bmatrix} \Delta X \\ \Delta Y \\ \Delta Z \end{bmatrix} + \begin{bmatrix} \pm I & \mp \Delta\kappa & \pm \Delta\varphi \\ \pm \Delta\kappa & \pm I & \mp \Delta\omega \\ -\Delta\varphi & \Delta\omega & I \end{bmatrix} \begin{bmatrix} x \\ 0 \\ -H \end{bmatrix} \qquad (7)$$

where,

- The top sign is valid for a system flying along the positive direction of the Y-axis (this flight line will be denoted as the forward strip), while the bottom sign is valid for a system flying along the negative direction of the Y-axis (this flight line will be denoted as the backward strip),
- $\Delta X, \Delta Y, \Delta Z$ are the components of the lever-arm offset vector $\vec{P}_G$,
- S is the scale factor for the mirror angle β (this scale factor should be unity for a bias-free system),
- H is the flying height above ground, and
- x is the lateral distance (with appropriate sign) between the LiDAR point in question and the projection of the flight trajectory onto the ground.

By utilizing the simplified LiDAR equation (Equation 7) in Equation 6 and rearranging the terms we get the final form of the simplified method equations (Equations 8 and 9 for strips flown in the same and opposite directions, respectively). In these equations, D is the difference between the lateral distance of conjugate points in strips A and B, $(x_A - x_B)$. D is a signed value that depends on the relationship between the involved strips. Therefore, the multiple signs ($\mp, \pm$) in equations 8 and 9 depend on the relationship between the strips, with the top sign used when strip A is to the right of strip B. One should note that for two flight lines, which are flown in opposite directions with 100% overlap, the expression in Equation 9 would reduce to the

form in Equation 10 (for such flight lines, D is equal to zero). The derived equations reveal the flight configuration that maximizes the impact and decouples systematic errors in the system parameters. For example, working with four strips which are captured from two flying heights in opposite directions with 100% overlap are optimal for the recovery of the planimetric lever-arm offsets as well as the boresight pitch and roll biases (Equation 10). In addition, two flight lines, which are flown in the same direction with the least overlap possible, are optimal for the recovery of the boresight yaw and roll biases, range bias, and mirror angle scale bias (Equation 8). Only a vertical bias in the lever-arm offset components cannot be detected by observing discrepancies between conjugate surface elements in overlapping strips. Such inability is caused by the fact that a vertical bias in the lever-arm offset components produces the same effect regardless of the flying direction, flying height, or scan angle. The inability of estimating the vertical bias in the lever arm components is not critical given the fact that the vertical lever-arm offset component can be determined with a very high accuracy by field survey. This has been confirmed by the fact that the quality of LiDAR data in the vertical direction is known to be much better when compared to the quality in the XY directions. Also, we can observe in the derived equations that the relationship between conjugate points in overlapping strips in the presence of biases in the system parameters is equivalent to a four-parameter rigid body transformation, i.e., three shifts (X_T, Y_T, and Z_T) and a rotation angle around the flight direction (ϕ) Equation 11. Once determined, the transformation parameters relating conjugate surface elements in overlapping strips can be expressed as a linear combination of the biases in the LiDAR system parameters. The resulting linear system can be then solved using a least-squares adjustment procedure to derive an estimate of the systematic biases in the data acquisition system.

$$\begin{bmatrix} X^A_{Bias} \\ Y^A_{Bias} \\ Z^A_{Bias} \end{bmatrix} = \begin{bmatrix} \mp D / H\ \delta\Delta\rho \mp D\ \delta S \\ \mp D\ \delta\Delta\kappa \\ \pm D\ \delta\Delta\varphi \end{bmatrix} + R_{(\pm \frac{2D}{H}\delta S)} \begin{bmatrix} X^B_{Bias} \\ Y^B_{Bias} \\ Z^B_{Bias} \end{bmatrix} \qquad (8)$$

$$\begin{bmatrix} X^A_{Bias} \\ Y^A_{Bias} \\ Z^A_{Bias} \end{bmatrix} = \begin{bmatrix} 2\ \delta\Delta X\ -\ 2\ H\ \delta\Delta\varphi \mp D / H\ \delta\Delta\rho \mp D\ \delta S \\ 2\delta\Delta Y\ +\ 2\ H\ \delta\Delta\omega \mp D\ \delta\Delta\kappa \\ 0 \end{bmatrix} + R_{(2\delta\Delta\varphi\ \pm\ \frac{2D}{H}\delta S)} \begin{bmatrix} X^B_{Bias} \\ Y^B_{Bias} \\ Z^B_{Bias} \end{bmatrix} (9)$$

$$\begin{bmatrix} X^A_{Bias} \\ Y^A_{Bias} \\ Z^A_{Bias} \end{bmatrix} = \begin{bmatrix} 2\ \delta\Delta X\ -\ 2\ H\ \delta\Delta\varphi \\ 2\delta\Delta Y\ +\ 2\ H\ \delta\Delta\omega \\ 0 \end{bmatrix} + R_{2\delta\Delta\varphi} \begin{bmatrix} X^B_{Bias} \\ Y^B_{Bias} \\ Z^B_{Bias} \end{bmatrix} \qquad (10)$$

$$\begin{bmatrix} X^A_{Bias} \\ Y^A_{Bias} \\ Z^A_{Bias} \end{bmatrix} = \begin{bmatrix} X_T \\ Y_T \\ Z_T \end{bmatrix} + R_\phi \begin{bmatrix} X^B_{Bias} \\ Y^B_{Bias} \\ Z^B_{Bias} \end{bmatrix} \qquad (11)$$

After estimating the biases in the system parameters ($\delta\hat{\Delta}X$, $\delta\hat{\Delta}Y$, $\delta\hat{\Delta}\omega$, $\delta\hat{\Delta}\varphi$, $\delta\hat{\Delta}\kappa$, $\delta\Delta\hat{\rho}$ and $\delta\hat{S}$), we can reconstruct the corrected point cloud using Equations 12 and 13 for forward and backward strips respectively. Since the system raw measurements are not available, the quantities presented in such equations are approximately determined. For instance, the lateral distances x_A and x_B are determined based on approximate centres of the scan-lines, while the mirror angles β_A and β_B are estimated using the average flying heights and the estimated lateral distances, i.e., -tan$^{-1}(x_A/H_A)$ and -tan^{-1} (x_B/H_B), respectively.

$$\vec{X}_{corr}^{A} = \vec{X}_{Bias}^{A} - \begin{bmatrix} \delta\hat{\Delta}X - H_A \,\delta\hat{\Delta}\varphi - \sin\beta_A\,\delta\hat{\Delta}\rho - H_A\beta_A\,\delta\hat{S} \\ \delta\hat{\Delta}Y + H_A\,\delta\hat{\Delta}\omega + x_A\,\delta\hat{\Delta}\kappa \\ -x_A\delta\hat{\Delta}\varphi - \cos\beta_A\,\delta\hat{\Delta}\rho - x_A\beta_A\,\delta\hat{S} \end{bmatrix} \qquad (12)$$

$$\vec{X}_{corr}^{B} = \vec{X}_{Bias}^{B} - \begin{bmatrix} -\delta\hat{\Delta}X + H_B\,\delta\hat{\Delta}\varphi + \sin\beta_B\,\delta\hat{\Delta}\rho + H_B\beta_B\,\delta\hat{S} \\ -\delta\hat{\Delta}Y - H_B\,\delta\hat{\Delta}\omega - x_B\,\delta\hat{\Delta}\kappa \\ -x_B\,\delta\hat{\Delta}\varphi - \cos\beta_B\,\delta\hat{\Delta}\rho - x_B\beta_B\,\delta\hat{S} \end{bmatrix} \qquad (13)$$

2.3 Quasi-rigorous Method

In the Quasi-rigorous method, the biases in the system mounting parameters are estimated in a single-step procedure while reducing discrepancies between conjugate surface elements in overlapping strips. It utilizes time-tagged point cloud and trajectory information. This method assumes that we are dealing with a linear scanner and that the LiDAR system unit is almost vertical. Such assumptions simplify the LiDAR geometric model as represented by Equation 1 to the form in Equation 14.

By utilizing the LiDAR model of the form in Equation 14 in Equation 6, we can get the final observation equation for the Quasi-rigorous method (Equation 15). Once the biases are recovered $(\delta\hat{\Delta}X, \delta\hat{\Delta}Y, \delta\hat{\Delta}\omega, \delta\hat{\Delta}\phi, \delta\hat{\Delta}\kappa, \delta\hat{\Delta}\rho, \delta\hat{S})$, we can reconstruct the corrected point cloud using Equation 16.

$$\vec{X}_G \approx \vec{X}_o + \begin{bmatrix} \cos\kappa & -\sin\kappa & 0 \\ \sin\kappa & \cos\kappa & 0 \\ 0 & 0 & 1 \end{bmatrix}\begin{bmatrix} \Delta X \\ \Delta Y \\ \Delta Z \end{bmatrix} +$$
$$+ \begin{bmatrix} \cos\kappa & -\sin\kappa & 0 \\ \sin\kappa & \cos\kappa & 0 \\ 0 & 0 & 1 \end{bmatrix}\begin{bmatrix} 1 & -\Delta\kappa & \Delta\varphi \\ \Delta\kappa & 1 & -\Delta\omega \\ -\Delta\varphi & \Delta\omega & 1 \end{bmatrix}\begin{bmatrix} -(\rho+\Delta\rho)\,sin(S\ \beta) \\ 0 \\ -(\rho+\Delta\rho)\,cos(S\ \beta) \end{bmatrix} \qquad (14)$$
$$= \vec{X}_o + \begin{bmatrix} \cos\kappa & -\sin\kappa & 0 \\ \sin\kappa & \cos\kappa & 0 \\ 0 & 0 & 1 \end{bmatrix}\begin{bmatrix} \Delta X \\ \Delta Y \\ \Delta Z \end{bmatrix} +$$
$$+ \begin{bmatrix} \cos\kappa & -\sin\kappa & 0 \\ \sin\kappa & \cos\kappa & 0 \\ 0 & 0 & 1 \end{bmatrix}\begin{bmatrix} 1 & -\Delta\kappa & \Delta\varphi \\ \Delta\kappa & 1 & -\Delta\omega \\ -\Delta\varphi & \Delta\omega & 1 \end{bmatrix}\begin{bmatrix} x \\ 0 \\ z \end{bmatrix}$$

$$\vec{X}_{Bias}^{A} - \vec{X}_{Bias}^{B} = \begin{bmatrix} (\cos\kappa_A - \cos\kappa_B)\delta\Delta X - (\sin\kappa_A - \sin\kappa_B)\delta\Delta Y \\ (\sin\kappa_A - \sin\kappa_B)\delta\Delta X + (\cos\kappa_A - \cos\kappa_B)\delta\Delta Y \\ 0 \end{bmatrix} +$$
$$+ \begin{bmatrix} (\sin\kappa_A z_A - \sin\kappa_B z_B)\delta\Delta\omega + (\cos\kappa_A z_A - \cos\kappa_B z_B)\delta\Delta\phi \\ -(\cos\kappa_A z_A - \cos\kappa_B z_B)\delta\Delta\omega + (\sin\kappa_A z_A - \sin\kappa_B z_B)\delta\Delta\phi \\ -(x_A - x_B)\delta\Delta\phi \end{bmatrix} +$$
$$+ \begin{bmatrix} -(\sin\kappa_A x_A - \sin\kappa_B x_B)\delta\Delta\kappa - [\cos\kappa_A \sin(S\beta_A) - \cos\kappa_B \sin(S\beta_B)]\delta\Delta\rho \\ (\cos\kappa_A x_A - \cos\kappa_B x_B)\delta\Delta\kappa - [\sin\kappa_A \sin(S\beta_A) - \sin\kappa_B \sin(S\beta_B)]\delta\Delta\rho \\ -[\cos(S\beta_A) - \cos(S\beta_B)]\delta\Delta\rho \end{bmatrix} +$$
$$+ \begin{bmatrix} (\cos\kappa_A z_A \beta_A - \cos\kappa_B z_B \beta_B)\delta S \\ (\sin\kappa_A z_A \beta_A - \sin\kappa_B z_B \beta_B)\delta S \\ -(x_A \beta_A - x_B \beta_B)\delta S \end{bmatrix} \qquad (15)$$

$$\vec{X}_{Corr} = \vec{X}_{Bias} - \begin{bmatrix} \cos\kappa\,\delta\hat{\Delta}X - \sin\kappa\,\delta\hat{\Delta}Y + \sin\kappa\,z\,\delta\hat{\Delta}\omega + \cos\kappa\,z\,\delta\hat{\Delta}\phi \\ \sin\kappa\,\delta\hat{\Delta}X + \cos\kappa\,\delta\hat{\Delta}Y - \cos\kappa\,z\,\delta\hat{\Delta}\omega + \sin\kappa\,z\,\delta\hat{\Delta}\phi \\ -x\,\delta\hat{\Delta}\phi \end{bmatrix} -$$
$$- \begin{bmatrix} -\sin\kappa\,x\,\delta\hat{\Delta}\kappa - \cos\kappa\,\sin(S\beta)\,\delta\hat{\Delta}\rho + \cos\kappa\,z\,\beta\,\delta\hat{S} \\ \cos\kappa\,x\,\delta\hat{\Delta}\kappa - \sin\kappa\,\sin(S\beta)\,\delta\hat{\Delta}\rho + \sin\kappa\,z\,\beta\,\delta\hat{S} \\ -\cos(S\beta)\,\delta\hat{\Delta}\rho - x\,\beta\,\delta\hat{S} \end{bmatrix} \qquad (16)$$

The procedure for estimating the necessary quantities $(x, z,$ and $k)$ presented in Equation 15 using the available data (time-tagged point cloud and trajectory positions), is as follows:

I. For a LiDAR point mapped at time (t), we search in the trajectory file for positions within a certain time interval $(t - \Delta t, t + \Delta t)$;

II. Then, a straight line is fitted through the selected trajectory positions to come up with a local estimate of the trajectory. After defining the local trajectory, the necessary quantities can be estimated as follows:

▪ x, which is the lateral coordinate of the laser point with respect to the laser unit coordinate system, can be determined by computing the normal distance (with the appropriate sign) between the LiDAR point and the interpolated trajectory data. The intersection of the normal from the LiDAR point to the interpolated trajectory will define the position of the trajectory at time t;

▪ z, which is the vertical coordinate of the laser point with respect to the laser unit coordinate system, can be determined by subtracting the elevation of the laser firing point (H) at time t, given by the interpolated flight trajectory, from the LiDAR point elevation (Z), i.e., $z = Z - H$; and

▪ κ, which is the trajectory heading, can be computed once we have the local estimate of the trajectory and its direction (defined by the neighbouring trajectory positions);

One should note that the established mathematical models for the two calibration methods are derived based on point primitives (i.e., conjugate points in overlapping strips). However, point-to-point correspondence in overlapping strips cannot be assumed due to the irregular nature of the LiDAR points. In this research, conjugate point and TIN patch pairs are used as primitives and the Iterative Closest Patch (ICPatch) procedure is applied to establish their correspondence. For more information regarding the ICPatch method, interested readers can refer to Habib et al., 2009a and Habib et al., 2010b. The utilization of conjugate point-patch pairs for the estimation of biases in the system parameters is accomplished through a weight modification for one of the points defining the TIN vertices (Habib et al., 2009b).

3. EVALUATION OF THE IMPACT OF THE CALIBRATION PROCEDURES

In this work, the impact of the proposed LiDAR system calibration procedures is analyzed through the evaluation of the relative and absolute accuracy of the LiDAR data before and after the calibration.

The impact on the relative accuracy will be assessed by quantifying the degree of compatibility between conjugate surface elements in overlapping strips before and after reconstructing the point cloud using the estimated system biases from both calibration methods. The compatibility will be evaluated by computing the 3D transformation parameters (discrepancies) between the overlapping strips before and after the calibration procedure. For the computation of the 3D transformation parameters, the ICPatch method is employed. The implementation details of this method can be found in Habib et al., 2009a and Habib et al., 2010b.
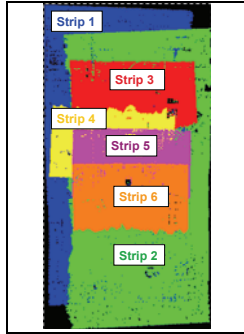
To evaluate the impact of the calibration procedure on the absolute accuracy of the point cloud, LiDAR linear and planar features will be used for the georeferencing of an image block covering the same area. The methodology used for photogrammetric georeferencing utilizing control linear and planar features is detailed in Shin et al., 2007. The absolute accuracy of the derived ground coordinates from the geo-

referenced image block is evaluated using a check point analysis.

4. EXPERIMENTAL RESULTS

4.1 Dataset Description

To evaluate the performance and test the validity of the proposed calibration methods, a LiDAR dataset captured by a Leica ALS50, which complies with the optimum flight configuration, was utilized. This configuration allows for the maximization of the impact of systematic biases and has the ability to decouple the different biases from each other. Figure 1 shows the characteristics of the acquired dataset and Table 1 presents the utilized overlapping strip pairs.

Strip Number	Flying Height	Direction
1	1150 m	N-S
2	1150 m	S-N
3	539 m	E-W
4	539 m	W-E
5	539 m	E-W
6	539 m	E-W

Figure 1. Dataset Configuration.

Table 1. Overlapping strip pairs used in the calibration procedure.

Overlapping Strips Cases	% of Overlap	Direction
Strips 1&2	80%	Opposite directions
Strips 3&4	25%	Opposite directions
Strips 4&5	75%	Opposite directions
Strips 5&6	50%	Same direction

4.2 Calibration Results

The estimated biases in the system mounting parameters using the two proposed calibration methods are presented in Table 2. It can be observed that quite compatible results are derived from the two methods. It can also be noted that a significant bias in the boresight roll angle was detected.

4.3 Impact Analysis

To check the impact of the calibration procedures on the absolute accuracy, LiDAR linear and planar features have been extracted and used for the georeferencing of an image block, which has been captured by a Rollei P-65 digital camera over the same area from two different flying heights (~550 and ~1200 m). The utilized camera has an array dimension of 8984x6732 pixels and a focal length of 60 mm. The quality of the derived ground coordinates from the geo-referenced image block was evaluated using a check point analysis. The results from the RMSE analysis for a total of 37 check points (GPS surveyed points) using the derived control linear and planar features from the LiDAR point cloud before and after using the two proposed calibration procedures are listed in Table 3. It can be noted that the results using planar features before the calibration are much worse than the results using linear

features. This might be due to the extraction process of the linear features, which are derived from the intersection of two planar patches (e.g., gable roofs). This extraction process might cancel the effect of some of the biases and reduce the data noise. The superior performance of the linear features after the calibration procedure might be due to the fact that the utilized patches had a relatively mild slope, which might reduce the reliability of the georeferencing results. Regardless of using linear or planar features significant improvement in the planimetric accuracy can be observed after the calibration for both methods. As expected, almost no improvement in the vertical accuracy is observed since detected biases in the system mounting parameters mainly affect the horizontal accuracy.

Table 2. Estimated system biases using the Simplified and the Quasi-rigorous methods.

Method	$\delta\Delta X$ (m)	$\delta\Delta Y$ (m)	$\delta\Delta\omega$ (")	$\delta\Delta\phi$ (")	$\delta\Delta\kappa$ (")	$\delta\rho$ (m)	δS
Simplified	0.03	-0.01	-26	-91	-19	0.18	0.000046
Quasi-rigorous	-0.01	0.02	-40.2	-90.9	-4.58	0.26	-0.000096

Table 3. RMSE analysis of the photogrammetric check points using extracted control linear features from the LiDAR data before and after using the two proposed calibration procedures.

	Before Linear/ Planar features	After	
		Simplified Method	Quasi-rigorous Method
		Linear/Planar features	Linear/Planar features
Mean ΔX (m)	-0.03/-0.36	-0.01/-0.10	-0.01/-0.09
Mean ΔY (m)	-0.18/0.67	0.06/0.24	-0.05/0.17
Mean ΔZ (m)	0.15/-0.05	-0.07/-0.15	0.11/-0.21
σ_X (m)	0.11/0.40	0.06/0.11	0.05/0.10
σ_Y (m)	0.15/0.29	0.08/0.06	0.06/0.07
σ_Z (m)	0.17/0.24	0.17/0.13	0.18/0.13
$RMSE_X$ (m)	0.11/0.53	0.06/0.14	0.05/0.13
$RMSE_Y$ (m)	0.23/0.72	0.10/0.24	0.07/0.18
$RMSE_Z$ (m)	0.23/0.25	0.18/0.20	0.21/0.25
$RMSE_{TOTAL}$ (m)	0.34/0.93	0.22/0.35	0.23/0.33

The impact of the proposed calibration procedures on the relative accuracy of the point cloud is evaluated by computing the discrepancies before and after the calibration procedure. The computed discrepancies are reported in Table 4. As observed in this table, the two methods provided compatible results. Also, a significant improvement can be observed, especially in the across flight direction between strips flown in opposite directions (X_T direction for strips 1&2, and Y_T direction for strips 3&4 and strips 4&5 – refer to highlighted cells in Table 4). This is expected since a larger bias was estimated in the boresight roll angle, which mainly affects the across-flight direction (i.e., constant shift across the flight direction and a rotation around the flight direction). Insignificant improvement can be observed for strips 5&6 in Table 4. This is due to the fact that for strips flown in the same direction the roll bias only causes a constant vertical shift between conjugate surfaces elements with a much smaller magnitude.

5. CONCLUSIONS AND RECOMMENDATIONS FOR FUTURE WORK

In this paper, two calibration methods have been introduced. The impact of the calibration procedures on the relative and absolute LiDAR point cloud accuracy was evaluated.

Table 4. Discrepancies between overlapping strips before and after applying the calibration parameters obtained using the Simplified and Quasi-rigorous methods.

Before Calibration			After Calibration					
			Simplified Method			Quasi-rigorous Method		
Strips 1&2			Strips 1&2			Strips 1&2		
X_T(m)	Y_T(m)	X_T(m)	X_T(m)	Y_T(m)	Z_T(m)	X_T(m)	Y_T(m)	Z_T(m)
1.10	-0.32	0.11	-0.01	-0.08	-0.05	0.11	0.07	-0.05
ω(deg)	φ(deg)	ω(deg)	ω(deg)	φ(deg)	κ(deg)	ω(deg)	φ(deg)	κ(deg)
0.0001	-0.052	0.0012	0.0006	-0.0027	-0.0045	0.0012	-0.0016	-0.0051
Strips 3&4			Strips 3&4			Strips 3&4		
X_T (m)	Y_T (m)	X_T(m)	X_T(m)	Y_T(m)	Z_T(m)	X_T(m)	Y_T(m)	Z_T(m)
0.18	0.41	-0.01	0.03	-0.26	0.00	-0.01	-0.01	0.01
ω(deg)	φ(deg)	ω(deg)	ω(deg)	φ(deg)	κ(deg)	ω(deg)	φ(deg)	κ(deg)
0.0484	-0.0005	0.0052	0.0053	0.0009	-0.0046	0.0052	0.0008	-0.0045
Strips 4&5			Strips 4&5			Strips 4&5		
X_T (m)	Y_T (m)	X_T(m)	X_T(m)	Y_T(m)	Z_T (m)	X_T(m)	Y_T(m)	Z_T(m)
-0.13	-0.58	0.07	0.04	-0.04	0.03	0.07	-0.04	0.03
ω(deg)	φ(deg)	ω(deg)	ω(deg)	φ(deg)	κ(deg)	ω(deg)	φ(deg)	κ(deg)
-0.0506	-0.0004	0.0039	-0.0019	0.0000	-0.0031	0.0039	-0.0001	-0.0054
Strips 5&6			Strips 5&6			Strips 5&6		
X_T (m)	Y_T (m)	X_T(m)	X_T (m)	Y_T(m)	Z_T(m)	X_T(m)	Y_T(m)	Z_T(m)
-0.06	-0.09	-0.05	-0.01	-0.19	0.02	-0.05	-0.03	0.03
ω(deg)	φ(deg)	ω(deg)	ω(deg)	φ(deg)	κ(deg)	ω(deg)	φ(deg)	κ(deg)
-0.0049	0.0014	0.0005	-0.0041	0.0003	0.0077	0.0005	0.0018	0.0076

Significant improvement in absolute and relative accuracy was obtained using the two proposed methods. Future work will focus on improving the computational speed of the proposed methods (e.g., parallel processing). Moreover, more testing with real data from operational systems will be performed.

REFERENCES

Bretar F., M. Pierrot-Deseilligny, and M. Roux, 2004. Solving the Strip Adjustment Problem of 3D Airborne Lidar Data. *Proceedings of the IEEE IGARSS'04,* 20-24 September, Anchorage, Alaska, 7, pp. 4734-4737.

Burman, H., 2000. *Calibration and Orientation of Airborne Image and Laser Scanner Data Using GPS and INS*. Ph.D. dissertation, Royal Institute of Technology, Stockholm. 125pages.

Crombaghs, M., E. De Min, and R. Bruegelmann, 2000. On the Adjustment of Overlapping Strips of Laser Altimeter Height Data. *International Archives of Photogrammetry and Remote Sensing*, 33(B3/1), pp. 230-237.

El-Sheimy, N., C. Valeo, and A. Habib, 2005. *Digital Terrain Modeling: Acquisition, Manipulation And Applications*. Artech House Remote Sensing Library. 257 pages.

Friess, P., 2006. Toward a rigorous methodology for airborne laser mapping. *Proceedings EuroCOW.* 25-27 January, Castelldefels, Spain. 7 pages (on CD-ROM).

Filin, S., 2001. *Calibration of spaceborne and airborne laser altimeters using natural surfaces*. PhD Dissertation. Department of Civil and Environmental Engineering and Geodetic Science, the Ohio-State University, Columbus, OH. 129 pages.

Filin, S. and G. Vosselman, 2004. Adjustment of Airborne Laser Altimetry Strips. *The International Archives of the Photogrammetry, Remote Sensing and Spatial Information Sciences*, 35 (B3), pp. 285-289.

Habib, A., K. Bang, A. P. Kersting, and D. C. Lee, 2009a. Error Budget of LiDAR Systems and Quality Control of the Derived Data. *Photogrammetric Engineering and Remote Sensing*, 75(9), pp. 1093–1108.

Habib, A., A. P. Kersting, K. I. Bang, and M. Al-Durgham, 2009b. A Strip Adjustment Procedure to Mitigate the Impact of Inaccurate Mounting Parameters in Parallel LiDAR Strips. *The Photogrammetric Record*, 24(126), pp. 171-195.

Habib, A., A. P. Kersting, and K. I. Bang, 2010a. Impact of LiDAR System Calibration on the Relative and Absolute Accuracy of the Adjusted Point Cloud, *EuroCOW Workshop on "Integrated Systems for Sensor Georeferencing and Navigation"*, Working Group 1/5, Spain.

Habib, A., A. P. Kersting, K. Bang, and D. C. Lee, 2010b. Alternative Methodologies for the Internal Quality Control of Parallel LiDAR Strips. *IEEE Transactions on Geoscience and Remote Sensing,* 48(1), pp. 221-236.

Kager, H., 2004. Discrepancies Between Overlapping Laser Scanning Strips- Simultaneous Fitting of Aerial Laser Scanner Strips. *Proceedings of the International Society for Photogrammetry and Remote Sensing XXth Congress*, Istanbul, 34(B/1): 555 - 560.

Kilian, J., N. Haala, and M. Englich, 1996. Capture and evaluation of airborne laser scanner data. *International Archives of Photogrammetry and Remote Sensing*, 31(B3):383–388.

Maas H. G., 2002. Method for measuring height and planimetry discrepancies in airborne laserscanner data. *Photogrammetric Engineering and Remote Sensing*, 68(9): 933–940.

Morin, K.W., 2002. *Calibration of Airborne Laser Scanners*. M.S. thesis, University of Calgary, Department of Geomatics Engineering. 125 pages.

Schenk, T., 2001. Modeling and Analyzing Systematic Errors in Airborne Laser Scanners, *Technical Report in Photogrammetry* No. 19, Ohio Sate University. 42 pages.

Shin, S., Habib, A., Ghanma, M., Kim, C., and Kim, E., 2007. Algorithms for Multi-Sensor and Multi-Primitive Photogrammetric Triangulation. *ETRI Journal*, 29(4), pp. 411-420.

Skaloud, J. and D. Lichti, 2006. Rigorous Approach to Bore-Sight Self-Calibration in Airborne Laser Scanning. *ISPRS Journal of Photogrammetry and Remote Sensing*, 61: 47–59.

Toth, C. K., 2002. Calibrating Airborne Lidar Systems. http://www.isprs.org/commission2/proceedings02/paper/084_100.pdf [Accessed: 15th November 2007].